Informes Técnicos Ciemat

1162
Febrero, 2009

Density Dependence of Particle Transport in ECH Plasmas ot the TJ-II Stellarator

V.I. Vargas
D. López-Bruna
J. Guasp
J. Herranz
T. Estrada
F. Medina
M.A. Ochando
J.L. Velasco
J.M. Reynolds
J.A. Ferreira
D. Tafalla
F. Castejón
A. Salas
and the TJ-II Team

Departamento de Fusión

Toda correspondencia en relación con este trabajo debe dirigirse al Servicio de Información y Documentación, Centro de Investigaciones Energéticas, Medioambientales y Tecnológicas, Ciudad Universitaria, 28040-MADRID, ESPAÑA.

Las solicitudes de ejemplares deben dirigirse a este mismo Servicio.

Los descriptores se han seleccionado del Thesauro del DOE para describir las materias que contiene este informe con vistas a su recuperación. La catalogación se ha hecho utilizando el documento DOE/TIC-4602 (Rev. 1) Descriptive Cataloguing On-Line, y la clasificación de acuerdo con el documento DOE/TIC.4584-R7 Subject Categories and Scope publicados por el Office of Scientific and Technical Information del Departamento de Energía de los Estados Unidos.

Catálogo general de publicaciones oficiales
http://www.060.es

Depósito Legal: M -14226-1995
ISSN: 1135 - 9420
NIPO: 471-09-016-9

Editorial CIEMAT

CLASIFICACIÓN DOE Y DESCRIPTORES

S29
ELECTRIC POWER; GUATEMALA; RURAL AREAS; GEOGRAPHIC INFORMATION SYSTEMS; RENEWABLE ENERGY SOURCESS; SUSTAINABLE DEVELOPMENT; ECONOMIC ANALYSIS

Density Dependence of Particle Transport in ECH Plasmas of the TJ-II Stellarator

Vargas, V.I.; López-Bruna, J.; Guasp, J.; Herranz, J.; Estrada, T.; Medina, F.; Ochando, M.A.; Velasco, J.L.; Reynolds, J.M.; Ferreira, J.A.; Tafalla, D.; Castejón, F.; Salas, A.; the TJ-II Team

20 pp. 14 fig. 40 ref.

Abstract:

We present the experimental dependence of particle transport on average density in electron cyclotron heated (ECH) hydrogen plasmas of the TJ-II stellarator. The results are based on: (i) electron density and temperature data from Thomson Scattering and reflectometry diagnostics; (ii) a transport model that reproduces the particle density profiles in steady state; and (iii) Eirene, a code for neutrals transport that calculates the particle source in the plasma from the particle confinement time and the appropriate geometry of the machine/plasma. After estimating an effective particle diffusivity and the particle confinement time, a threshold density separating qualitatively and quantitatively different plasma transport regimes is found. The poor confinement times found below the threshold are coincident with the presence of ECH-induced fast electron losses and a positive radial electric field all over the plasma.

Dependencia del Transporte de Partículas con la Densidad en PLasmas ECH del Stellarator TJ-II

Vargas, V.I.; López-Bruna, J.; Guasp, J.; Herranz, J.; Estrada, T.; Medina, F.; Ochando, M.A.; Velasco, J.L.; Reynolds, J.M.; Ferreira, J.A.; Tafalla, D.; Castejón, F.; Salas, A.; the TJ-II Team

20 pp. 14 fig. 40 ref.

Resumen:

Presentamos la dependencia experimental entre transporte de partículas y densidad promedio en plasmas hidrogénicos del stellarator TJ-II con calentamiento ciclotrónico electrónico (ECH).
Basamos los resultados en: (i) datos de densidad y temperatura de los diagnósticos de esparcimiento Thomson y reflectometría; (ii) un modelo de transporte que reproduce los perfiles estacionarios de la densidad de partículas; y (iii) Eirene, un código de trasporte de neutros que calcula la fuente de partículas del plasma según su tiempo de confinamiento y las geometrías apropiadas de máquina y plasma. Tras estimar una difusividad efectiva de las partículas y su tiempo de confinamiento, se encuentra una densidad umbral entre regímenes de transporte cualitativa y cuantitativamente distintos. Bajo el umbral se encuentran tiempos de confinamiento pobres coincidiendo con la presencia de pérdidas de electrones rápidos inducidas por el ECH y con un campo eléctrico radial positivo en todo el plasma.

1. *Introduction*

An acknowledged difficulty for the estimation of particle transport in magnetic fusion machines is obtaining the source terms. The neutrals distribution, for example, can be important over a large part of the plasma column at least in toroidal sectors such as the gas puffing zone or the surroundings of limiters. In machines with small traverse dimensions and large areas of plasma-wall closeness, like the TJ-II, the recycling fluxes can represent the main particle source term. On the other hand, studying the behaviour of the particle transport with different external controls is not less important than studying the thermal conduction. The latter has been done traditionally in many devices and also in the TJ-II from the global [**1**] and local [**2**] perspectives. Now we want to extend these studies to the particle transport.

Transport in plasmas is not necessarily determined following a purely diffusive paradigm. Cross-field advection of plasma structures [**3**] or, from a general theoretical viewpont, the statistical properties of transport step-sizes [**4**], can give rise to non-diffusive features. Therefore, the flux of the transported magnitude is not simply proportional to its gradient. Still, the use of *effective* transport coefficients as in Fick's law is a very convenient way to quantify transport properties: it eases the interpretation of results and the comparison among different devices. The use of effective transport coefficients is therefore commonly found in experimental works.

Particle transport in stellarators has been less studied than in tokamaks. Earlier transport studies using the particle balance method in the W7-AS stellarator indicate that, at least in the density gradient region, the diffusion coefficient D scales positively with the heating power and negatively with the magnetic field B, the rotational transform ι and the density n_e [**5**, **6**, **7**, **8**]. In particular, some of the plasmas studied in [**5**] (see also [**6**]) can be compared with ours: using the particle balance method and relying on calculations of the neutrals transport, the particle diffusivity in ECH plasmas (350 kW, X-mode; $B = 1.2$ T) yielded diffusivities decreasing with density in the density gradient region. The minimum values, found far from the edge, were estimated to be around 0.5 m^2/s. Of course, these values decreased considerably for $B = 2.5$ T confining fields.

More recent particle transport experiments in the W7-AS [**9**] and LHD [**10**] stellarators have been carried out with the gas modulation method. In the first, the experiments were performed at various values of the plasma density, although always considerably larger than those of the TJ-II. The particle diffusion was found to scale roughly in inverse proportion to the plasma density, which was compatible with previous studies. In the case of LHD, the values of D and the radial convection velocity v are studied with emphasis on the possible relationship with microturbulence. These and other studies have intended to uncover the physics dominating particle (and heat) transport, which requires performing parametric scans in a given confinement mode.

Several particle transport studies have been carried out in the TJ-II following different approaches (see [**11**, **12**] and references therein). During the first TJ-II experimental campaigns, plasmas were produced in all metal (stainless steel) wall conditions instead of boronized wall, as it pertains to the present work. Particle confinement times τ_p were obtained based upon density profiles in the scrape-off layer (SOL) from lithium beam measurements, which allowed obtaining e-folding lengths and an estimation of diffusion in the SOL. For plasma conditions otherwise comparable to those later discussed, confinement times were found roughly in the range from 5 ms to 15 ms depending on the power-per-particle ratio: the higher this ratio, the lower τ_p [**15**]. It was by then pointed out that the role of ECH-induced direct losses in conditions of high magnetic ripple had to be considered, at

least in studies of energy balance. A systematic impurity particle transport study was later done with boron-coated walls using silicon tracer ions and several types of radiation detectors to estimate confinement times from the decay of the signals [**16**]. Density, ECH power and magnetic configuration scans were performed. A sharp increment of impurity confinement was identified above line-density values that depended (although not strongly) on magnetic configuration. A strong dependence of the impurity confinement time was found, however, on the heating power [**17**, **12**]. For those cases closer to our present conditions (same configuration, similar ECH power ≈ 400 kW and hydrogen plasma), the density scan yielded confinement times of the silicon ions between 3 ms ($\bar{n} = 0.3 - 0.4 \times 10^{19}$ m^{-3}) and close to 20 ms ($\bar{n} = 0.6 - 0.7 \times 10^{19}$ m^{-3}).

In this paper we return to the problem of particle transport in TJ-II ECH hydrogen plasmas using particle balance methods. Unfortunately, the small magnetic field ($B = 1$ T) of the device limits the plasma density range in such plasmas considerably, but a density scan is still pertinent. The experimental data consist of plasma electron temperature and density profiles in stationary conditions. The electron source profile is calculated with Eirene, a comprehensive Monte-Carlo code for neutrals transport, following an iterative process that we summarize here:

(1) We introduce a guessed particle confinement time, τ_p, in a version of the Eirene code [**13**] adapted to the conditions of the TJ-II red (see reports in [**14**]) and benchmarked against ECH discharges to match CX spectra, to calculate the particle source distribution due to recycling and puffing. The geometry of the vacuum chamber and the magnetic configuration are fully considered. For conciseness we shall hereafter call our adaptation of the Eirene code simply Eirene.
(2) The source is used in a transport model that reproduces the experimental steady state density profile after tuning a few parameters, thus giving a new τ_p.
(3) The updated τ_p is used again to obtain a new source, which is re-set in the particle balance and the process returns iteratively to point (i) until a steady state that matches the experimental density profile is obtained red for the given τ_p and source returned by Eirene.

Note that, in this process, the relationship between τ_p and source is embedded in Eirene, but this relationship *only matches the steady state one after reaching convergence* in the iterations. Once the source (and τ_p) is estimated, the effective electron diffusivity can be obtained.

Our results are based on a set of 27 TJ-II discharges obtained by selecting from a density scan those discharges that suit the above procedure best. The conditions are fairly restrictive for the following reasons: a calculation of the recycling fluxes takes τ_p as one of its main input parameters; our experience, both in controlling the density in TJ-II discharges and in our previous estimates and calculations [**19**], is that recycling (expressed through a recycling factor R) closes a feedback loop in the particle balance such that the system is, when $R \approx 1$, quite unstable. To avoid a long argument, let us make the simplest analysis of particle balance, $\partial_t n = -\nabla \cdot \mathbf{\Gamma} + S$, where n is the electron density, S the particle source from recycling and $\mathbf{\Gamma}$ the electron radial flux. Integrating to the plasma volume we obtain an equation for the total particle number N, that is, $\partial_t N = -\Gamma A + \Gamma_N A$; where Γ_N represents the influx of electrons, due to recycling, through the plasma surface whose area is A. Then, if $\Gamma_N = R\Gamma$, and we make the electron outflux depend on the confinement time, $\Gamma \sim N/\tau_p$, we have an evolution equation with growing or decaying exponential behaviour depending on whether $R > 1$ or $R < 1$,

$$\frac{\partial N}{\partial t} \propto \frac{(R-1)}{\tau_p} N. \tag{1.1}$$

Obviously, things are quite more complicated than this analysis since R, τ_p and Γ are interrelated, but in Eq. 1.1 the referred two important pieces of the problem are highlighted: τ_p and R. Both are, in principle, unknown in our problem and the present work is aimed at obtaining an estimate of the experimental electron diffusion under the conditions that best lead to knowing R and τ_p. If we can experimentally fix R to a known value (≈ 1 in our case), we may rely on the Eirene calculations and the stationariness of the plasmas to work out τ_p from the iterative procedure enumerated above. This is what we detail in what follows. We start (Section 2) with a description of the discharges that have been selected from the TJ-II database, which includes the criterion to fix values for R. The model used to reproduce the density profiles and thus obtain τ_p is given in Sec. 3. The results are presented in Sec. 4 and discussed in Sec. 5. The work is summarized in Section 6.

2. *Experimental data*

The 27 discharges here analyzed correspond to a density scan in TJ-II ECRH plasmas. Two gyrotrons focussed at the magnetic axis provide a net heating power of about 400 kW on plasmas with line density $\approx 0.5{-}0.8{\times}10^{19}$ m^{-3}. The configuration yields a plasma volume of 1.1 m^3 and edge rotational transform $\iota_a = 1.65$ with very low vacuum magnetic shear.

Data from gas puffing diagnostics have been recorded for all of the discharges in the experimental set. After pre-filling the vacuum chamber, the typical puffing waveform for a constant density discharge consists of an initial and short pulse to reach the optimum pressure for plasma breakdown [**18**], followed by a rather constant (normally slowly decreasing) puffing rate during the discharge. An example is given in figure 1, where we also show the smoothed signal of a micro-wave diode installed inside one of the quasi-optical transmission lines. We have used these gas puffing rates at the time of Thomson Scattering measurement as input in the Eirene calculations. All discharges in this study have the poloidal limiters at the last closed flux surface (LCFS) or more retired from the plasma, so they can be considered to be limited by the groove of the vacuum chamber that protects the helical and central conductors (helical limiter). The working gas in all cases is hydrogen. Soft X-Ray emissions indicate that the impurity contribution to the electron density n_e is about 10%, mainly due to C and B. Contributions from heavier impurities are usually negligible in TJ-II ECRH plasmas, and particularly in those pertaining to this work.

An important parameter in the calculations is the recycling factor. We have chosen discharges for which we can set arguably $R = 1$. The choice is based on the experience that the wall saturation limit is reached in the TJ-II after some 5 to 15 discharges [**20**] depending on the initial wall conditioning. As indicated also in Ref. [**20**], the ratio between the H_α monitors intensity and the line averaged density can be used as an indicator of the recycling conditions: when this ratio saturates to a certain value (which depends on the H_α monitor), recycling is $R \approx 1$. Therefore, comparable wall conditions for the disharges of the scan, in terms of H saturation, is ensured upon saturation of this quotient in the corresponding experimental day. Fig. 2 shows the evolution of $H_\alpha/\bar{n}$ during one day for discharges that correspond to a density scan. The lines mark a saturation level for different H_α monitors. Data represented with dots come from a monitor looking at one of the poloidal limiters of the TJ-II. The other two, represented with squares and diamonds, correspond to monitors looking at the groove of the vacuum chamber in different toroidal sectors. The groove acts as a helical limiter concentrating most of the plasma-wall interaction, thus giving a global view of recycling. Only discharges above saturation have been chosen for the analysis.

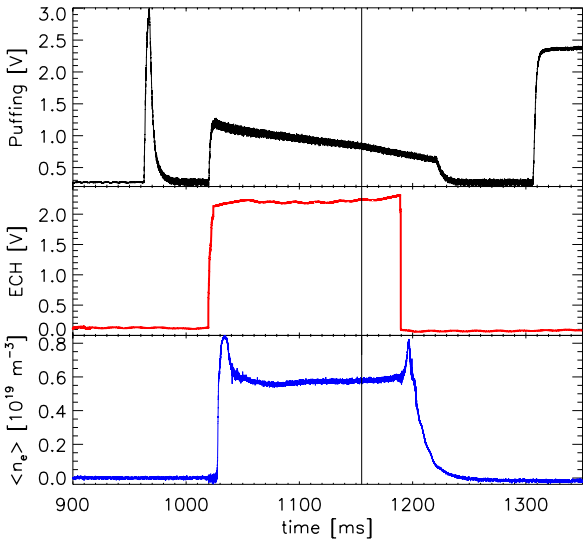

FIGURE 1. *Gas puffing signal (top), electron cyclotron heating (middle) and line density (bottom) in a typical TJ-II ECH discharge. The time of TS firing is marked with a vertical line.*

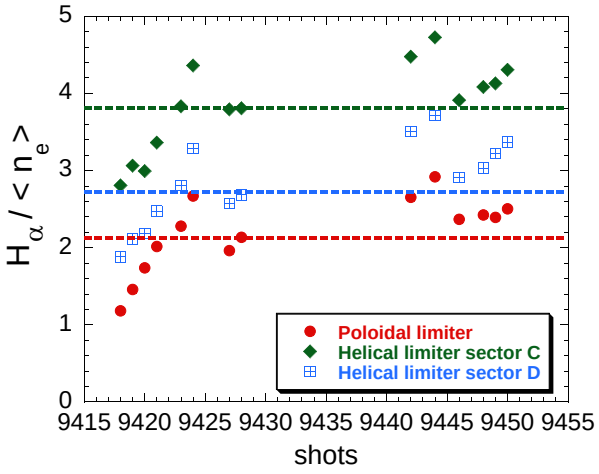

FIGURE 2. *Evolution of the ratio $H_\alpha/\bar{n}$ for different H_α monitors during an experimental day. Shown are discharges that correspond to a density scan. Horizontal lines indicate reference saturation levels for which $R \approx 1$.*

Once the discharges from the density scan were chosen to match the criteria above, their density and electron temperature profiles measured using the Thomson Scattering diagnostic (TS) were read from the TJ-II database. The density profile was completed with reflectometry data [**25**]. The procedure to build the profiles for the analysis has been described in an earlier work [**2**]. In brief, T_e is taken directly from the TS diagnostic after smoothing and n_e is taken from TS after smoothing and re-scaling in such a way that the line density, obtained when the TS profile is continued with reflectometry data, matches the experimental line average obtained

from the interferometer. Fig. 3 shows electron density and temperature profiles of the present study, which are commonly found in TJ-II ECH plasmas.

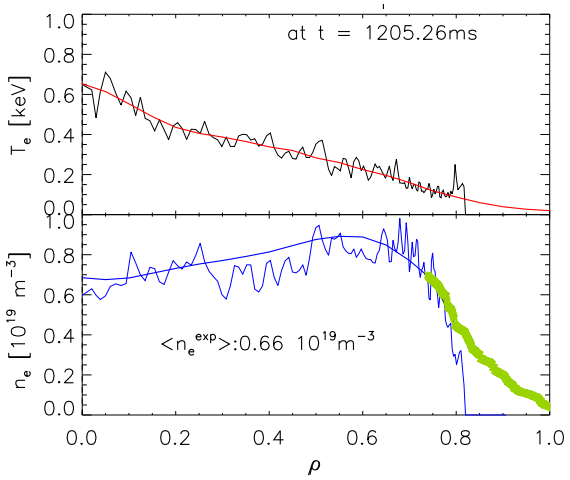

FIGURE 3. *Top: T_e profile from Thomson Scattering and smoothed profile used in the analysis. Bottom: n_e from TS (thin line), from reflectometry (thick line) and smooth profile used in the analysis after matching and re-scaling to the experimental line density for TJ-II discharge #9444.*

In this work we need estimates of gradients. In order to extract error bars for the radial derivatives based on the experimental data we have several possibilities, all of them artificial to a certain degree because of the spatial discreteness of the diagnostics. Moreover, when a diagnostic like TS gives a fair amount of radial density of data, the evaluation of gradients from raw data is very disperse as can be deduced from figure 3. We make the working assumption that the smoothed profiles are a good representation of the profiles that, on average, correspond to the steady state part of a given discharge and, in addition, that their variability is dominated by the accidental errors, that is, by the variability among discharges. In what follows, we shall express the errors associated with gradients as statistical deviations from repetitions of the experiments.

3. *Estimate of the particle source*

As mentioned in the Introduction, we use an adaptation of the Eirene code [**14**] for the characteristics of the TJ-II to obtain the particle source distribution due to recycling and external gas puffing.

τ_p and R are important input parameters for the calculations. Since the discharges have been selected so as to ensure $R \approx 1$, we need a criterion to establish the confinement time. From previous works we know that τ_p improves noticeably with density [**15**] even within the range of densities below the ECH cut-off limit ($\approx 1.7 \times 10^{19}$ m^{-3}; corresponding to line averaged density $\bar{n} \approx 1.2 \times 10^{19}$ m^{-3}). In particular, in early studies in metal wall conditions [**21**, **22**] it was found that τ_p ranges from ≈ 5 ms in the low density cases to some 15 ms in high density discharges. Despite our plasmas having different wall conditions, we could use an interpolation of these values to estimate particle source profiles assuming that they are compatible with a steady state for the given experimental density and temperature profiles. We

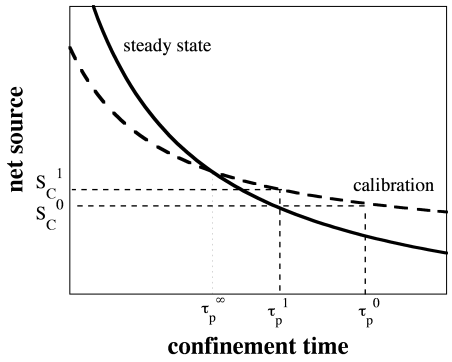

FIGURE 4. *Scheme of iteration process red at constant density N.*

should keep in mind, however, that the source returned by Eirene does not need to be the one that solves the steady-state transport equation *for any confinement time*. The source returned by the code is the one that suites a "calibration" or benchmarking process guided by TJ-II experimental values. In other words, Eirene gives a relationship between τ_p, plasma profiles and recycling source –maybe with the addition of external gas puffing. Let us make a zero-dimensional simplification of the problem to fix ideas: let S_C be the net source yielded by Eirene for a plasma with N particles. Then the calibration is a relationship $S_C = S_C(\tau_p, N)$. On the other hand, the steady state relationship between those numbers is $S_S = N/\tau_p$. The equation $S_C = S_S$ may have in principle different solutions for τ_p, or maybe none if N is too far from the values chosen for calibration. In figure 4 we plot an ideal case in which there is one solution. If we start with an initial guess τ_p^0, the code returns a source S_C^0 that does not match the steady state τ_p^1. Then we can, maintaining S_C^0, use a transport code that returns the new steady state confinement time τ_p^1. From this confinement time (and always keeping the experimental N) we obtain a new source S_C^1 and so forth until we *converge* to the solution point τ_p^∞. Of course, in a general case τ_p^∞ can be an unstable point of the iterative map that yields either *divergence* or convergence to a different solution. For all the discharges analyzed in this work we have found that the iterative process converges towards a unique solution, at least when starting with reasonable confinement time values. To verify convergence, in most discharges we have repeated the iterative process starting with quite different values of τ_p above and below the converged one.

In reality, the input data to Eirene consist of three-dimensional distributions of plasma parameters and realistic boundaries, so the iterative process is actually done in a high dimensional space of which figure 4 is a simplification. As noted at the beginning of this section, we are taking the correct calibration of Eirene as a working hypothesis. Once verified that we have convergence, we simply acknowledge that the obtained confinement times are our best *numerical* estimate of the particle source for the TJ-II in the plasmas here studied. A comparison with τ_p values obtained from previous experiments, as we shall comment later, indicates that the τ_p calculated are in fair agreement with the experiments. Thus, we can conversely consider our iterative process as a way to check the benchmarking of Eirene against general ECRH plasmas of the TJ-II stellarator; but now we can use the radial particle sources obtained from the iterative process to estimate radial profiles of effective diffusivities.

3.1. *Transport model*

The transport model is not important in the sense that it is only used to reproduce the experimental profiles in each iteration step. Therefore the transport model does not need to be based on physical grounds. Despite this, we have used forms that can be identified with physical effects. In the iterative process we make the particle balance evolve towards steady state characterized by $\nabla \cdot \mathbf{\Gamma} = S$ for a particle flux $\mathbf{\Gamma} = -D\nabla n + n\mathbf{v}$ that we tune changing a few parameters as we explain in what follows. All the transport analysis has been done with the ASTRA system [**23**].

There are two main plasma regions where the direct losses $\mathbf{v}$ are supposed to be important in ECH plasmas of the TJ-II: the heating deposition zone, near the magnetic axis; and the outer plasma near the LCFS. In the former zone, we should consider the known pump out processes, experimentally identified in the first TJ-II campaigns [**15**]. However, this is also a zone of very difficult treatment. As a matter of fact, flat or hollow density profiles are a common feature of low density ECH plasmas in stellarators. In addition, thermodiffusion may have some relevance in this core region, as suggested in tokamaks [**26**] and stellarators [**27**]. We exclude this zone from our calculations of D. However, we still keep the pump out term because, as discussed in Ref. [**15**], a reduction of the pump out fluxes does alter the density profiles and we want to reproduce them entirely so that the distribution of the electron source be properly evaluated. Since our description of transport is one-dimensional, the spatial dependence in the transport code is expressed in terms of a radial coordiante ρ, or normalized flux surface label. Thus, the pump out term is $n(\rho)v_p(\rho)$ where $v(\rho)$ is simply a Gaussian where we can vary the centering, width and height. Since the pump out happens in the flatter region of the density profiles, with this choice the flux $n(\rho)v_p(\rho)$ is approximately Gaussian.

The direct losses near the LCFS are obtained with a smooth step-like analytical function $v_d(\rho)$ such that there is a radial drift $v_d(\rho)$ for minor radii above some value ≈ 0.85. We include such term because the transport description near the LCFS based solely on diffusion yields extraordinarily large diffusivities. In addition, previous [**28**] and recent [**29**] calculations suggest that transport in the region $\rho \gtrsim 0.85$ would be better described with average radial drifts on the order of several m/s. As is also the case with v_p, this function $v_d(\rho)$ is used to ease reproducing the experimental steady density profile; particularly, we move its centering and height until the density of the plasma edge region is reproduced in steady state. Typically, the centering is moved from $\rho = 0.88$ for low density discharges to $\rho = 0.92$ for the high density cases.

We have so far considered radial drifts in the transport description. To obtain the diffusive term we use the following formulae for the particle and electron-heat diffusivities:

$$D = C_1 + C_2 f_t^2 \chi \tag{3.1}$$

$$\chi = C_3 + C_4 \nu_e \rho^2 f_t^3, \tag{3.2}$$

where the C_i are constants, ν_e is the electron collision frequency and $f_t \propto \sqrt{\rho}$ is the fraction of trapped particles. We write our transport coefficient D in this way so the reader can identify the dependencies with the anomalous transport based on trapped electron instabilities proposed in Ref. [**31**], although there is no evolution of the electron temperature. Note that we are adding an offset in χ and D through the constants C_1 and C_3.

3.2. *Effective diffusivity*

Let us obtain an effective diffusivity based on the flux surface-averaged particle source, density gradient and convective terms. If we take the volume V enclosed

by a flux surface as a "radial" coordinate, the balance between particle source and particle flux is

$$S(V) = \frac{\mathrm{d}}{\mathrm{d}V} \langle \mathbf{\Gamma} \cdot \nabla V \rangle \,, \tag{3.3}$$

from where we can easily obtain a relationship between the volume integral of the source, S_I, and the "radial" flux $\Gamma = nv - D_e(\partial n/\partial\rho)\,|\nabla\rho|$. Here we assume that v is a flux surface averaged drift velocity, or pure convection. Considering that all our magnitudes are given in the variable ρ, working out D_e from the integral of Eq. 3.3 yields

$$D_e(\rho) = -\frac{S_I - V'nv\,|\langle\nabla\rho\rangle|}{V'n'\left\langle(\nabla\rho)^2\right\rangle}. \tag{3.4}$$

As usual, a prime indicates derivative with respect to ρ; and the gradients are flux surface averages $\langle\cdots\rangle$ evaluated for the vacuum configuration, not very different from the equilibrium one in these low pressure plasmas. Eq. 3.4 is the expression we shall use to obtain an effective diffusivity. However, it must be recalled that we are using a transport model to make the evolving profiles converge towards the experimental ones. Albeit similar, the converged density profile is generally not identical to the experimental one as can be seen in the example of Fig. 5, where both are shown along with the resulting particle source. The converged profile is only used to obtain a converged τ_p and S_e, but D in equation equation 3.4 is obtained using the experimental density profile.

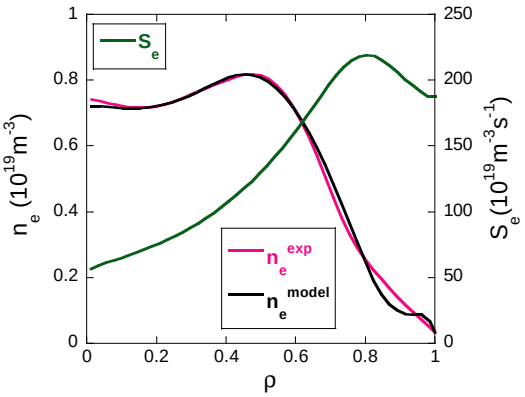

FIGURE 5. *Experimental and converged electron densities (left); and electron source term (right) in the particle balance for TJ-II discharge #9427 ($\bar{n}_e = 0.58 \times 10^{19}\ m^{-3}$).*

3.3. *Source and confinement time*

In equation 3.4, the net particle source S_I depends strongly on recycling or, in the frame of our model, on the particle confinement time

$$\tau_p = \frac{\int_0^1 nV'\mathrm{d}\rho}{S_I}.$$

The practical procedure to determine both, source and confinement time simultaneously, has been delineated above. After having described the transport model, let us recall the procedure in more concrete terms:

(1) We start with the experimental profiles and a guessing $\tau_p \approx 8$ ms.
(2) The new particle source is calculated and returned to the transport evolution.
(3) A few parameters are changed in the transport model so the evolving profiles tend towards the experimental ones. There is then a new confinement time.
(4) The process is repeated returning to (ii) until convergence is found, i.e., until there is no need to change parameters in the transport code to obtain the experimental profiles using the source calculated with Eirene.

The electron temperature is fixed in the process. The transport particle balance equation is evolved during a time comparable to τ_p before returning the numerical flow to Eirene with an updated τ_p. The number of iterations is ~ 10. Slightly different confinement times are found depending on the matching between calculated and experimental density profiles. From the repetitions of the calculations to ensure convergence, we have obtained different values of τ_p and source that allow obtaining statistical deviations.

4. *Results*

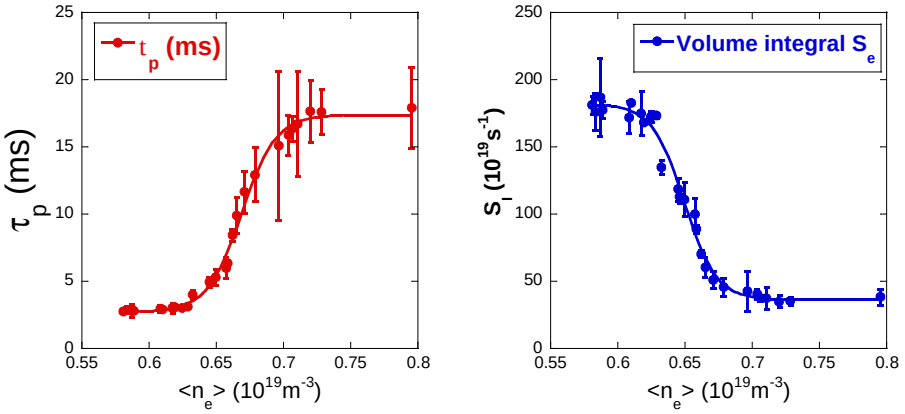

(a) (b)

FIGURE 6. *Particle confinement time (a) and volume integral of the particle source (b) as a function of the line-averaged density for a set of 27 stationary ECRH discharges of the TJ-II. The continuous lines represent fits to a hyperbolic tangent function.*

Fig. 6.a contains the particle confinement times found for the density scan. They are found between 2.74 ms and 17.93 ms and show two distinct confinement regimes separated by a threshold. To define such threshold numerically we have chosen the formula

$$\tau_p = \frac{a+b}{2} + \frac{a-b}{2} \tanh\left(5\frac{c-\bar{n}_e}{d}\right), \tag{4.1}$$

with $\bar{n}_e$ in units of 10^{19} m^{-3}; from which we obtain $a = 2.8 \pm 0.2$, $b = 17.3 \pm 0.3$, $c = 0.670 \pm 0.001$ and $d = 0.12 \pm 0.01$ (the resulting fitting function is plotted in Fig. 6.a). The choice of this function responds to the observed fact that the density dependence of τ_p is small above or below the threshold defined by the parameter c, that is, $\bar{n}_{th} \approx 0.67$. Fig. 6.b shows the corresponding integrals of the particle source. In general, $S_e(\rho)$ presents a maximum around ρ=0.8, as observed also in other ECRH plasmas in stellarators [**9**], a direct consequence of the penetration of

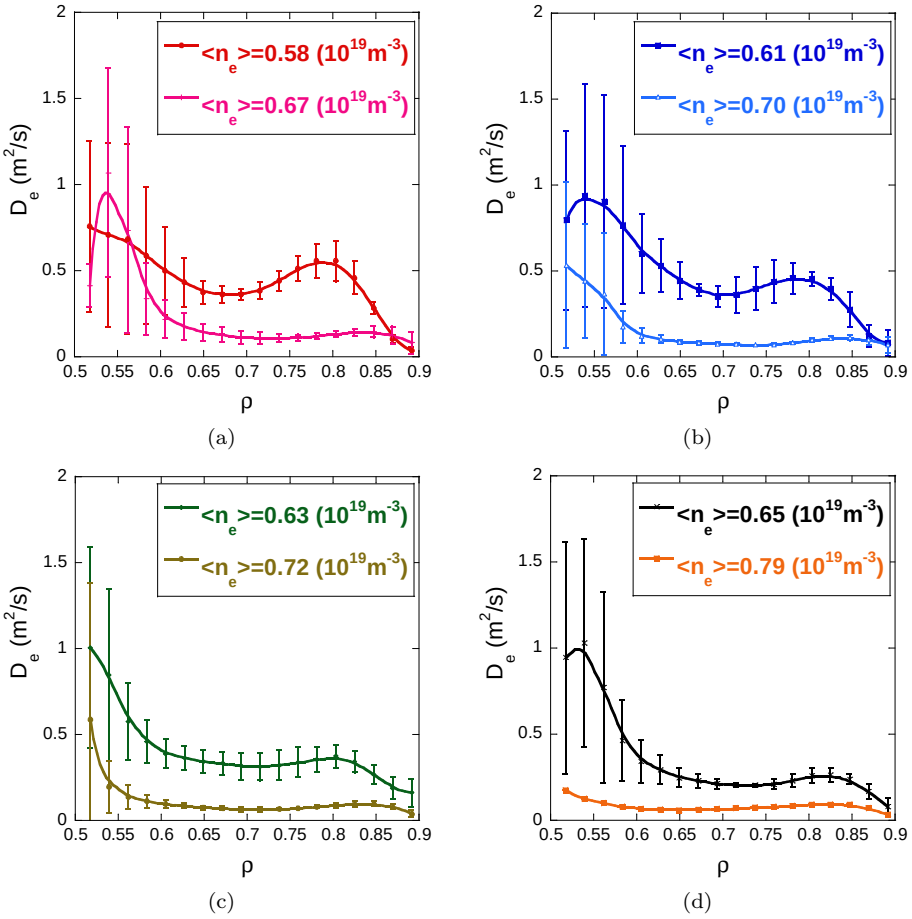

FIGURE 7. *Average profiles of electron effective diffusivity: a)* $\bar{n}_e = 0.58 \times 10^{19}\ m^{-3}$ *and* $\bar{n}_e = 0.67 \times 10^{19}\ m^{-3}$*, b)* $\bar{n}_e = 0.61 \times 10^{19}\ m^{-3}$ *and* $\bar{n}_e = 0.70 \times 10^{19}\ m^{-3}$*; c)* $\bar{n}_e = 0.63 \times 10^{19}\ m^{-3}$ *and* $\bar{n}_e = 0.72 \times 10^{19}\ m^{-3}$*; d)* $\bar{n}_e = 0.65 \times 10^{19}\ m^{-3}$ *and* $\bar{n}_e = 0.79 \times 10^{19}\ m^{-3}$*. Standard deviation is represented with vertical bars.*

the neutrals. The numerical values found for τ_p will be compared with those found in previous studies, although our main interest hereafter focuses on the existence of a threshold density separating low and high values.

The D_e-profiles are studied mainly in the region where $v_p + v_d$ is a small contribution to the particle flux in comparison with the diffusive part. The region of interest is then $0.5 < \rho < 0.9$, i.e., most of the density gradient region. The results are presented as profiles averaged in groups of close densities. We formed 8 groups of 3 or 4 discharges from which an average profile and standard deviation were obtained. Figures 7 show $D_e(0.5 \leq \rho \leq 0.9)$ from such average profiles and the corresponding standard deviations. From (a) to (d), the figures show profiles for several line-densities. The standard deviation is larger near $\rho = 0.5$, where the density gradient approaches zero. Close to $\rho = 0.9$, standard deviations should not be trusted because the true contribution of $v_d(\rho)$ cannot be established with our means.

A synoptic view of the dependence of D_e with $\bar{n}$ can be found in figure 8, where contour maps obtained by linear interpolation of the discrete averaged data are

shown. Fig. 8.a and figure 8.b are, respectively, D_e as obtained from equation 3.4 and the net effective diffusivity obtained with $v = v_p + v_d = 0$, so the reader can see the influence of these radial drifts on our D_e by comparing them. Obviously, only v_d is of importance in the range $0.5 \leq \rho \leq 0.9$ and its effect consists of lowering D_e near the edge because only a part of the transport can be ascribed to D_e when there is convection. The furrow in figure 8.b moving outwards up to $\rho \approx 0.75$ is due to the maximum density gradient moving likewise, as can be seen in figure 8.c. We have also indicated that the vacuum magnetic configuration used in this density scan has the low order rational rotational transform $\iota = n/m = 8/5$ located in $\rho = 0.77$, which we indicate with a continuous horizontal line. To know whether or not the location of the maximum gradient is related to the presence of this low order rational we should repeat the study with different magnetic configurations.

In figure 9 we plot cuts of figure 8 at several radii in the density gradient region with their fittings to another hyperbolic-tangent function. The inflexion points of the curve fits are always located in the range $\bar{n}_e = 0.63 - 0.66 \times 10^{19}$ m^{-3}.

The modelling of v_d is not completely arbitrary. Aside from its usage to help in reproducing the experimental profiles, the steady-state values obtained are comparable to those found with the orbit-following code ISDEP [**29**]. In these calculations, a large number of particles are launched inside the plasma with a Gaussian distribution function in velocity space and a spatial distribution based on the density profile. The guiding-center trajectories are followed in a collisional background based on the electron and ion temperature profiles. The net flow through different flux surfaces is computed and divided by the corresponding density to obtain an effective radial drift velocity. In figure 10, such calculations are done in a thermal bath of typical ECH-plasma temperature profile with density profiles similar to those used in this work. Since the electrostatic plasma potentials affect transport considerably, the calculations have included profiles based on the experimental ones [**30**]. The resulting v_d profiles show that the effective velocity moves outwards for higher densities and larger values are reached for smaller densities. Of course, these calculations do not distinguish between diffusive or convective processes and account only for collisional losses. A qualitative agreement is found between results, as well as the same order of magnitude in the values. With this figure we show that, with a kinetic treatment, the effective radial drift velocity is meaningful in the region where we are describing most of the transport with v_d. Moreover, the kinetic calculations show non-diffusive features, which indicates that convective fluxes are of major importance in the confinement global behaviour in the long mean-free-path regime. Again, these results are meant to support the choice of a radial drift in our modelling although our discussion does not depend on them.

5. *Discussion*

The results shown above indicate a clear transition between two particle confinement regimes. To discuss these results, let us first find what is different in the input to the calculation of the source. For this, we observe (figure 11) that the source from recycling is in all cases much larger than the particle source from gas puffing, as expected from $R \approx 1$ discharges. Taking for simplicity the cases in which gas puffing fluxes are zero, the volume integral of the source in steady state is given by the integrated outgoing particle flux in a way that only depends on plasma profiles. The data in figure 8 show that the confinement improvement coincides with the increasing density gradient. At more or less the threshold density, the maximum density gradient stays in the same position corresponding to the higher confinement regime. We make this more explicit in figure 12, where we plot the average values of D_e with respect to $\mathrm{d}n_e/\mathrm{d}\rho$ for a chosen radial position, $\rho = 0.75$. In principle, this is

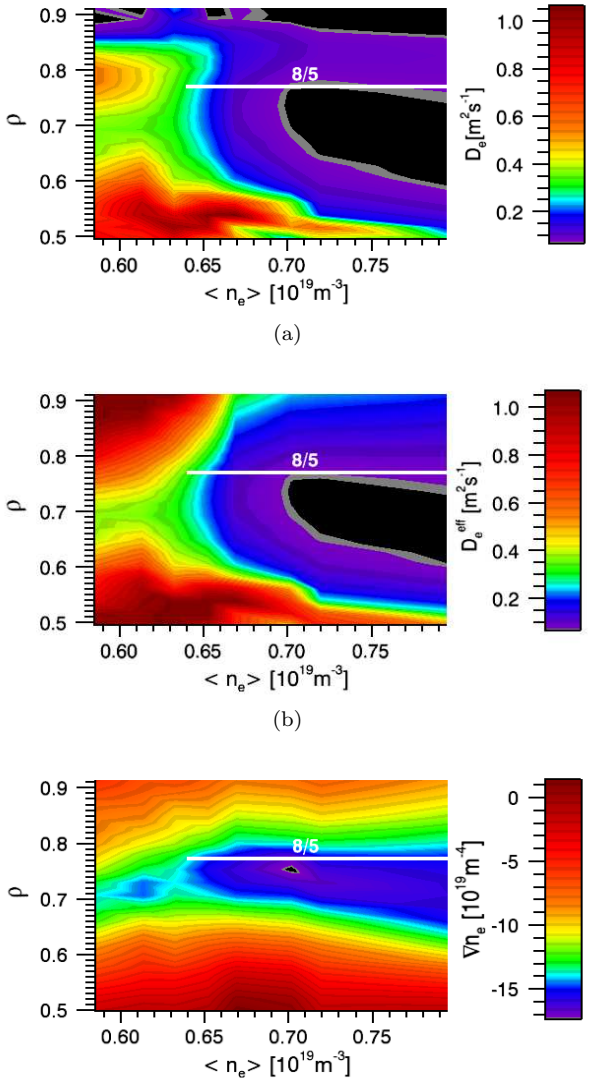

FIGURE 8. *Contour maps of: (a) D according to equation 3.4; (b) an effective diffusivity taking $v = 0$ in equation 3.4; and (c) the density gradient in the radial interval $0.5 \leq \rho \leq 0.9$. A horizontal line marks the location of the low order vacuum magnetic resonance $\iota = n/m = 8/5$. Areas in black are below scale.*

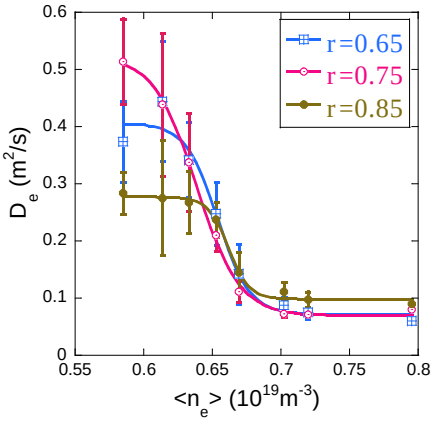

FIGURE 9. *Average electron diffusivities as a function of line-averaged density for several radii in the density gradient region: ρ=0.65 (squares); ρ=0.75 (dot-circles) and ρ=0.85 (filled circles). Bars represent statistical deviation.*

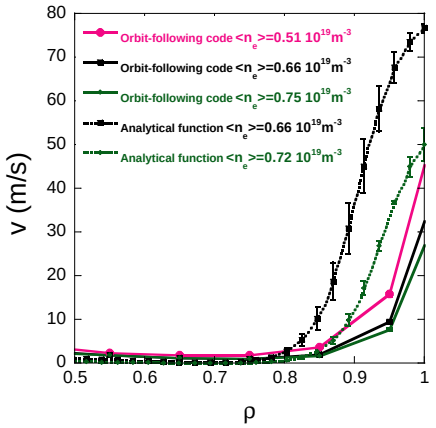

FIGURE 10. *Effective velocities obtained with ISDEP for different line densities and comparison with the profiles found to match the experimental discharges in the particle balance.*

nothing but the obvious assert that a small diffusivity gives rise to large gradients. However, if there is such a notable change in confinement we must expect a significant one in the intensity of H_α light for the same scan. This is the case in figure 13, where the data of H_α normalized by the line-average density corresponds to the set of analyzed discharges. The different markers correspond to the H_α monitors presented in figure 2. Other (not shown) monitors with different viewing geometries show similar trends. Let us keep in mind that the H_α signal is affected by several factors that involve the density profiles themselves and the solid angle of collected light coming from quite different lines-of-sight. Even so, the general trend can be identified: in the low confinement region, the signal is higher in response to the higher outflux; in the region of changing τ_p there is an inverse trend, corresponding to the change in confinement. Fewer data are available in the higher density range because the density control is difficult above the threshold density when $R = 1$ because of the ECH cut-off, somehow corresponding to Eq. 1.1, but the $H_\alpha/\bar{n}$ val-

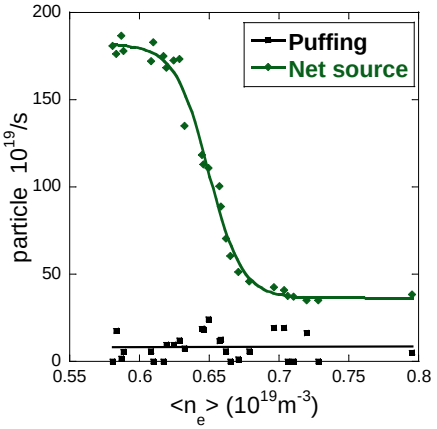

FIGURE 11. *Net particle fluxes coming from gas puffing (squares) and recycling (diamonds) for all the discharges of the density scan.*

ues are found to remain low. The diagnostic is then compatible with the results of figure 6, especially because the TJ-II is quite a large aspect-ratio machine: small changes in surface-related magnitudes (like fluxes) can have a notable impact in volume-integrated magnitudes.

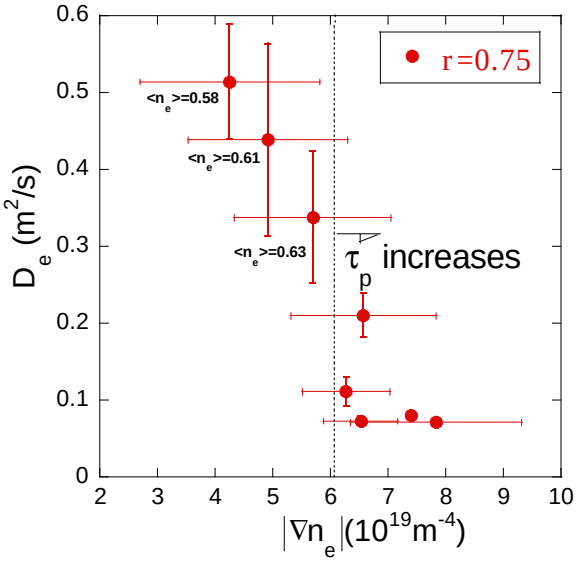

FIGURE 12. *Effective diffusivity at $\rho = 0.75$ as a function of the density gradient in the same position.*

Let us now look for differences among the plasmas above/below the density threshold. For low densities the confinement times are small and, above a density threshold (given the ECH power), the calculated τ_p increases roughly five-fold to what we may call "normal" values. The exact values shown in figure 6 are not as important as the qualitative trend, but we know from the experiments that

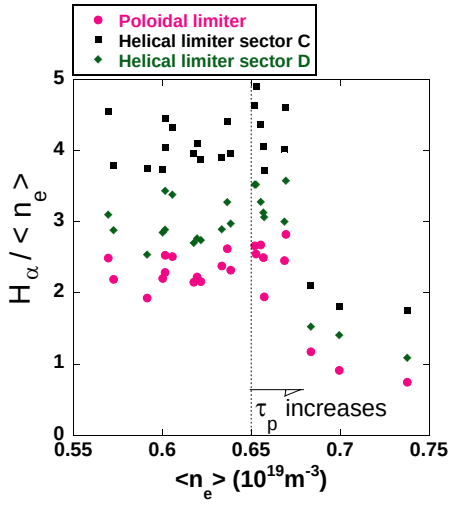

FIGURE 13. *Intensity of the H_α signals (arbitrary units) divided by the line density around the Thomson Scattering measurement time for discharges belonging to the density scan. Shown are H_α monitors looking at the poloidal (circles) and helical (squares and diamonds) limiters.*

such values are reasonable [**15**, **16**, **17**]. Now, it is worth recalling that the *energy* confinement time for the electrons in this density range increases linearly with line-average density from, roughly, 2 to 3 ms [**32**]. Looking at figure 6 we realize that τ_p in the region of poor confinement approaches these values, a suggestion of confinement regime dominated by kinetic effects. If this is the case, we expect that the hottest species (electrons) will find its way out of the confining volume more easily than the much cooler and collisional ions, a situation that can give rise to a positive radial electric field E_r in most of the plasma. A review of TJ-II literature shows that this is indeed the case [**12**, **33**, **34**]: data from the Heavy Ion Beam Probe (HIBP) diagnostic installed in the machine have allowed identifying a density threshold for the appeareance of $E_r < 0$ in the plasma. The electrostatic plasma potential profiles are monotonically decreasing for low densities but present a minimum, near the plasma edge, for line-densities above $0.5 - 0.7 \times 10^{19}$ m^{-3} in the same magnetic configuration now studied. This minimum, which moves inwards as the density increases [**35**], corresponds to a change of sign of the electric field and is often referred to as "shear layer" or "inversion layer" because the macroscopic $E \times B$ flows reverse sign at that location. Data obtained with probes in the plasma edge region confirm the HIBP results: the inversion layer in comparable plasmas shows up when $\bar{n}_e \approx 0.6 \times 10^{19}$ m^{-3} [**36**].

Above the density threshold, which we now identify with the inversion of electric field sign not far from the edge, the diffusivity decreases notably corresponding to the augmented τ_p. However, the maximum density gradient apparently stays in more or less the same position above the threshold, while the region with $E_r < 0$ extends throughout the plasma as found experimentally in Ref. [**35**] with reflectometry measurements. Therefore the density gradient is not a cause of the further changes in electric field above the threshold density.

What is the agent that drives the change in E_r using the density as control parameter? The electron temperature plays a crucial role in determining the particle fluxes, and in the $1/\nu$ regime these fluxes decrease as the density increases. ECH plasmas of the TJ-II exhibit direct losses of electrons with toroidal and poloidal

asymmetries, as expected from the different drift velocities in the different magnetic ripple wells [**34**, **37**, **38**]. But not only the thermal population is affected by collisionality: suprathermal electrons generated in the ECH deposition zone can escape the plasma very rapidly due to their trapping in the structure of magnetic mirrors of the magnetic configuration or, else, escape to other toroidal locations where they can likewise bounce rapidly and also convect out of the plasma. Fig. 14 illustrates these notions by showing the X-ray flux signal in the 20 to 200 keV range, corresponding to discharges of our scan. This signal originates after impact of the particles in the limiter and can be interpreted as a monitor of fast particle losses. A fit to the data using the same function as for figure 9 shows a similar density threshold, $\bar{n} \approx 0.62$. Most likely, it is not a density but a power-per-particle threshold with some contribution of the magnetic configuration because (apart from ι-profile effects) the magnetic ripple is linked to the plasma size. Quantifying the contribution of different ingredients (e.g. the modification of the distribution function in the ECH heating zone, the direct losses associated to trapping fraction, the total power convected by these electrons and their outflow) is difficult, but the qualitative effect is well known from TJ-II experiments. For example, in Ref. [**39**] the soft X-ray spectra revealed a strong deformation of the electron energy distribution function in a regime of high ripple losses in plasmas with densities slightly below 0.6×10^{19} m^{-3}, and in Ref. [**40**], input power density scan experiments led to establish the coupling between the characteristic energy of the electron suprathermal tail and plasma potential, i.e., the higher the energy of the electron suprathermal tail the higher plasma core potential.

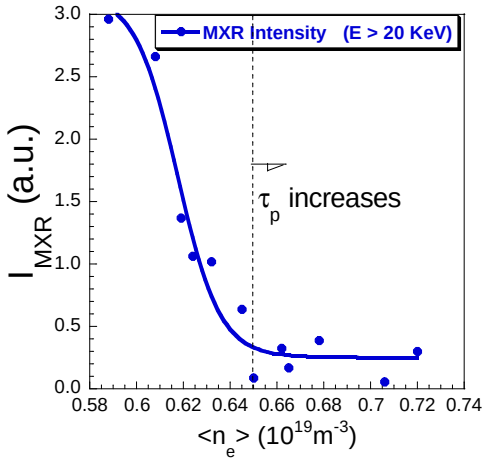

FIGURE 14. *Integrated MXR emission (> 20 keV) for several discharges belonging to the density scan, as a function of the line-averaged density. The line is a fitting function.*

In the end, and before dedicated analysis and measurements are performed, direct losses of high energy electrons seem to be responsible for having $E_r > 0$ all over the plasma, a condition that is coincident with very poor particle confinement times. Different mechanisms can avoid this situation, one of them being the increase of plasma density, as done in the present scan. Other means are lowering the heating power density, forcing the change in electric field with biasing or changing the magnetic configuration. All of them have been actually tried with the TJ-II. The strong power-per-particle dependence of τ_p claimed in Refs. [**15**] and [**17**] is also found with the particle balance method and the values of τ_p are similar for similar

conditions. In any case, particle confinement time studies in ECH plasmas must watch for the possibility of involving different plasma states like those shown here.

6. *Summary*

Stationary hydrogen discharges of the TJ-II Heliac with boronized wall have been analyzed within the ECH density range to obtain effective particle diffusivities and particle confinement times. The calculations are based on the Eirene code for neutrals transport adapted to the characteristics of the machine. The strong plasma wall interaction couples the particle source to the plasma state in the studied conditions of high recycling. Two particle transport regimes can be clearly identified, separated by a density threshold if ECH and magnetic configuration are fixed, as shown independently by several diagnostics, particularly H_α monitors, X-rays, reflectometers, Langmuir probes and HIBP. The low confinement state is coincident with positive radial electric fields in the whole plasma and with the presence of ECH-driven fast escaping electrons, and the confinement times approach electron energy confinement times. The effective diffusivities are large in the density gradient region, around 0.5 m^2/s. The particle confinement time increases sharply when the radial elecric field is no longer positive in the entire plasma and then the maximum density gradient increases and moves outwards, in correspondence with a much smaller effective diffusivity in the same region (~ 0.1 m^2/s). The confinement times found are comparable to those obtained in metalic wall plasmas [**15**] and from tracer impurities in boronized wall [**17**].

Acknowledgements

The authors wish to acknowledge the interest and advise of Dr. B. van Milligen during the preparation of this paper. The work has been partially supported by the Spanish "Ministerio de Educación y Ciencia".

References

1. Ascasíbar E *et al.* 2005 Nucl. Fusion **45** 276
2. Vargas V I *et al.* 2007 Nucl. Fusion **47** 1367
3. Krasheninnikov S I, Smolyakov A I, Soboleva T K 2005 Phys. Plasmas **12** 0072502
4. Calvo I, Sánchez R, Carreras B A, van Milligen B Ph, 2007 Phys. Rev. Lett. **99** 230603
5. Sardei F *et al.*, *Particle transport and recycling studies on the WVII-AS stellarator*, in Controlled Fusion and Plasma Heating (Proc. of the 17th Eur. Conf. Amsterdam), Vol. 14B, Part II, European Physical Society, Genova (1990) 471.
6. Ringler H *et al.* 1990 Plasma Phys. Control. Fusion **32** 933
7. Weller A *et al.* 1991 Plasma Phys. Control. Fusion **33** 1559
8. Maassberg H *et al.* 1993 Plasma Phys. Control. Fusion **35** B319
9. Koponen J P T *et al.* 2000 Nucl. Fusion **40** 365
10. Tanaka K *et al.* 2006 Nucl. Fusion **46** 110
11. Alejaldre C *et al.* 2001 Nucl. Fusion **41** 1449
12. Hidalgo C *et al.* 2005 Nucl. Fusion **45** S266
13. Reiter D, Baelmans M, Börner P 2001 Fusion Sci. Technol **47** 172.
14. Reiter D *The Eirene Code User Manual*, Version: 11/2005; http://www.eirene.de.
15. Tabarés F L *et al.* 2001 Plasma Phys. Control. Fusion **43** 1023
16. Zurro B *et al.* 2004 Rev. Sci. Instruments **75** 4231
17. Zurro B *et al. Impurity transport and confinement in the TJ-II stellarator*, 20th IAEA Fusion Energy Conference 1 - 6 November 2004, Vilamoura, Portugal.
18. Cappa A, Castejón F, Tabarés F L, Tafalla D, *et al.* 2001 Nucl. Fusion **41** 363
19. López-Bruna D, Ferreira J A, Tabarés F L, Castejón F, Guasp J, *Simulación dinámica del reciclado y de la inyección de partículas en los plasmas del TJ-II*, Ciemat Technical Report No. 1099, February 2007.
20. Ferreira J A, Tabarés F L, Tafalla D, *Particle balance in TJ-II plasmas under boronized wall*

conditions, Proc. of the 32nd EPS Conf. on Contr. Fusion and Plasma Phys., Tarragona, 27 June – 1 July 2005, ECA Vol. 29 C P-4.009 (2005).
21. Tabarés F L *et al.*, *Plasma edge studies and particle control in the TJ-II stellarator*, Proc. of the 26th EPS Conf. on Contr. Fusion and Plasma Physics, Maastricht, 14-18 June 1999, ECA Vol. 23 J (1999) 369
22. Tabarés F L *et al.*,Vacuum **52** (1999) 11
23. Pereverzev G V, Yushmanov P N, *ASTRA Automated System for TRansport Analysis*, Max-Planck-Institut für Plasmaphysik, Rep. IPP 5/98, Garching, February 2002.
24. Tabarés F L *et al.* 2001 J. Nucl. Mater. **290–293** 748
25. Estrada T *et al.* 2001 Plasma Phys. Control. Fusion **43** 1535
26. Weisen H, Furno I, TCV Team 2001 Nucl. Fusion **41** 1227
27. Stroth U *et al.* 1999 Phys. Rev. Lett. **82** 928
28. Guasp J, Liniers M 2000 Nucl. Fusion **40** 397
29. Castejón F *et al.* 2007 Plasma Phys. Control. Fusion **49** 753
30. Krupnik L *et al.* 2005 Czech. J. Physics **55** 317
31. Kadomtsev B B, Pogutse O P 1971 Nucl. Fusion **11** 67.
32. Vargas V I, López-Bruna D, Herranz J, Castejón F Ciemat Tecnical Report No. 1079, July 2006.
33. Ascasíbar E *et al.* Plasma Phys. Control. Fusion **44** B307
34. Sánchez J *et al.* 2007 Nucl. Fusion **47** S677
35. Estrada T *et al.* 2006 Nucl. Fusion **46** S792
36. Pedrosa M A *et al.* 2005 Plasma Phys. Control. Fusion **47** 777
37. Ochando M A *et al.* 2006 Fusion Sci. Technol. **50** 313
38. Medina F *et al.* 2007 Plasma Phys. Control. Fusion **49** 385
39. Ochando M A *et al.* 2003 Plasma Phys. Control. Fusion **45** 223
40. Medina F *et al. Electron distribution function and radial electric fields in the TJ-II stellarator* 31st EPS Conference on Plasma Phys. London, 28 June - 2 July 2004 ECA Vol. 28G, P-4.182 (2004)